

Article

# Magnetic Field Effects on Thermal Nanofluid Flowing through Vertical Stenotic Artery: Analytical Study

Ramzy Abumandour<sup>1</sup>, Islam M. Eldesoky<sup>1,2</sup>, Mohamed Abumandour<sup>3,\*</sup>, Kareem Morsy<sup>4,5</sup>  
and Mohamed M. Ahmed<sup>1</sup>

- <sup>1</sup> Basic Engineering Sciences Department, Faculty of Engineering, Menoufia University, Shebin El-Kom 32511, Egypt; ramzy\_abumandour@sh-eng.menofia.edu.eg (R.A.); islam\_eldesoky@sh-eng.menofia.edu.eg (I.M.E.); m.ahmed@sh-eng.menofia.edu.eg (M.M.A.)
- <sup>2</sup> Basic Sciences Department, Elmenofia Higher Institute of Engineering and Technology, Bagour 32821, Egypt
- <sup>3</sup> Department of Anatomy and Embryology, Faculty of Veterinary Medicine, Alexandria University, Alexandria 21544, Egypt
- <sup>4</sup> Biology Department, College of Science, King Khalid University, Abha 62529, Saudi Arabia; k.morsy@yahoo.com
- <sup>5</sup> Zoology Department, Faculty of Science, Cairo University, Cairo 12613, Egypt
- \* Correspondence: M.abumandour@alexu.edu.eg; Tel.: +20-10-0032-2937

**Abstract:** The present investigation represents the first complete illustration of nanofluids flow. The effectiveness of wall slip and heat transfer on magnetohydrodynamic nanofluids flow over porous media in vertical stenotic artery with catheter has been analyzed. By considering the long-wavelength with low-Reynolds number approximation, a mathematical solution was derived to velocity, stream function, pressure difference, and temperature. The nanoparticle's concentration, amplitude ratio, catheter size, and flow rate have been used to extract the pressure difference. This study analyzes the interaction effect of slip and thermal conditions on nanoparticles fluid suspension with a catheter in a vertical stenotic artery with/without the presence of magnetic field and porosity. The results are helpful for understanding the role of the engineering applications of nanofluids in biomedicine and some other applications. The results of this paper reveal that the nanoparticles concentration has little effect on the velocity, and the concentration, slipping, and porosity of the nanoparticles decreases the thermal energy.

**Keywords:** nanofluids flow; vertical stenotic artery; velocity



**Citation:** Abumandour, R.; Eldesoky, I.M.; Abumandour, M.; Morsy, K.; Ahmed, M.M. Magnetic Field Effects on Thermal Nanofluid Flowing through Vertical Stenotic Artery: Analytical Study. *Mathematics* **2022**, *10*, 492. <https://doi.org/10.3390/math10030492>

Academic Editor: Petr Knobloch

Received: 10 November 2021

Accepted: 20 December 2021

Published: 3 February 2022

**Publisher's Note:** MDPI stays neutral with regard to jurisdictional claims in published maps and institutional affiliations.



**Copyright:** © 2022 by the authors. Licensee MDPI, Basel, Switzerland. This article is an open access article distributed under the terms and conditions of the Creative Commons Attribution (CC BY) license (<https://creativecommons.org/licenses/by/4.0/>).

## 1. Introduction

On account of their huge applications in many fields, in this paper we concentrate on the more prominent disciplines of engineering: industrial and biomedical. To improve the thermo-physical properties of the fluids, nanometer particles are injected into them. Several materials can be used to make nanoparticles, such as minerals (gold, silver, ferric, aluminum, copper), nitride ceramics (SiN, AlN), carbide ceramics (SiC, TiC), oxide ceramics (Al<sub>2</sub>O<sub>3</sub>, CuO), single, double, or many carbon nanotubes (DWCNTs, SWCNTs, MWCNTs), and semiconductors (TiO<sub>2</sub>). Basic fluids after injection with these nanoparticles are defined as nanofluids. In general, rigid bodies have major thermo-physical properties comparison with traditional thermo-fluids influence, such as water, oil, and ethylene glycol viscosity, thermoconductance, thermodiffusion, and convective overheat transfer coefficients for these fluids, which are improved by injecting nanoparticles into them. Therefore, the potency of nanofluids in many applications have attracted more and more attention.

In this portion, we will be going to record some applications of nanofluids, such as biomedical applications (antibacterial activity, nanodrug delivery, cancer therapeutic, cryopreservation, nanocryosurgery, molecular imaging and photothermal therapy, ultrasonic

image, guided therapy, and MRI imaging). Nanofluids have not been solely applied to the area of biomedicine, but they have been used for distinct bioindustrial engineering areas such as heat transfer intensification (electronic applications, microelectronics, transportation brake and other vehicular nanofluids, manufacture refrigeration implementations, warming houses and reducing defilement, nuclear devices refrigeration, space and defense technologies, pharmaceutical processes, smart fluids, and extraction of geothermal power and other energy sources), mass transfer enhancement, energy apps (power buffering, heliacal sucking), mechanistic apps (friction minimal, magnetohydrodynamic stamping), and other applications (intensification micro-reactors, transportation braking, microbial fuel cell, nanofluids with unique optical properties, nanofluid detergent) [1–7].

In some instances, the spread of cholesterol in blood vessels blocks the blood, which coagulating inside the cordial artery, deemed as a porous media, [6,8,9]. Chu and Fang [3] considered Newtonian fluid boundary conditions. The effect of slip conditions at the boundary was taken into consideration in the analytical solutions for complex geometries, which have been introduced by Hron et al. [10].

The combined effects between the electrical conductivity of the nanofluids and traditional fluids during the influence of magnetic field and heat transmit overhead convectively heated surfaces is used in engineering and industrial applications. This phenomenon is termed “MHD”, where the magnetic fields can motivate the moving conductive fluid to produce the currents. Due to the induced current, there is a difference in the magnetic field and generating forces on the fluid. Every unit of volume moving through an electric field and magnetic field exposed to a force is known as the Lorentz force [10–12]. MHD fluid flows require the augmentation between Navier Stokes equation of fluid dynamics and Maxwell’s equation of electromagnetism. Analytically or numerically, these differential equations have been solved.

The combined impact of the thermic and peristaltic effects is exceedingly employed in numerous applications to determine the sensitiveness of thermic viscosity [13,14]. The influence of MHD and wall properties through the peristaltic inflow of a Jeffrey nanofluid during duct has been explored [15]. The researchers discussed the mathematical analysis to the influx and the heat transfer. Several significant parameters were examined on the materialistic quantities of the inflow during schemes for Jeffrey and Newtonian fluids. It has been detected that to the Jeffrey fluid, the inflow rate and thermic impact is smaller than that of the Newtonian fluid. In addition, it has been discovered that increasing the concentricity of the nanoparticle leads to a decrease in the velocity and temperature.

For the time being, the impacts of heat transmit together with entropy propagation have been discovered due to the distinguished results by Bejan [16]. Compound integration for entropy propagation and different effects such as friction forces, alchemical reactions, and viscosity lead to more losses of energy in the thermodynamics framework. The entropy propagation performs a renowned pivotal role in various industrial procedures including alchemical vapor sedimentation tools, turbine mechanization, burning, heat exchangers, solar collectors, and refrigeration instruments. Khan and Ali [17] discussed the modern evolutions for modelling and emulation to entropy propagation for dispersed material using self-stimulation. Numerous authors [18–21] have dedicated their searches for studying entropy propagation for different nonlinear inflow and heat transmit models.

For the time being, nanoscale particles are used in solar energy models because of their thermic advantages. The creation of useful products such as photocatalysts, organic pollutants for minimal concentricity, electrical energy manufacture, and ecological reconquest is due to its powerful oxidizing strength and prolonged stabilization [22,23]. Zeiny et al. [24] presented a crossbred nanofluid founded on solar thermic transmutation competence. Then, they introduced the photothermal transmutation efficiency by Beer’s law. For the time being, most of the researchers focus their search for nanofluids based on nanoparticles with a high thermic conductivity to maximize the heat transmit rate efficiency and to control the heat transmit by using the magnetic field. Shi et al. [25] presented a combination of  $\text{Fe}_3\text{O}_4$  and  $\text{TiO}_2$  nanoparticles to supply with the cleaning and separating circuit. Furthermore,

they made a comparison to separate the Fe<sub>3</sub>O<sub>4</sub> and TiO<sub>2</sub> nanoparticles at various values of the magnetic field. Prakash et al. [26] have improved the performance of the theoretical micropump for the solar MHD peristaltic nanofluid.

In fact, the heat transmit performs a necessary function in acquiring knowledge of the properties of biological tissues. Truly, the mutual analysis around the peristaltic and heat transmit are significant for blood thermodynamic characteristics in processes such as oxygenation and hemodialysis, cancer therapy, and hyperthermia [27–29]. These joint impacts of heat and mass transmit are important in several types of manufacturing, such as chemical, food, paper, and metallurgical. For further details, see [30–37].

The goal of this paper is to analyze the MHD Newtonian fluid with the effect of heat transfer on nanofluid in an annulus tube with porous medium, considering the slip effects at the wall. This paper is being arranged as follows. Part 1 consists of the modeling problem and the formulation of governing equations with non-dimensional parameters. In part 2, the settling of the problem with the long-wavelength and Low-Reynolds number approximation is presented. The results are then discussed with the previous published data.

**2. Materials and Methods**

*Mathematical Formularization*

We impose a viscous nanofluid flow into an asymmetrical circuitous tube with a mean radius  $R_0$ . The shear stress is proportional to the velocity gradient, which is known as the Newtonian fluid. Taking the flexibility of the tube walls into consideration, the existence of stenosis makes them fixed. A symmetrical rigid catheter of radius  $a_1$  is implemented. Movement of fluid is caused by the pressure difference at the compliant wall of the tube, as shown in Figure 1.

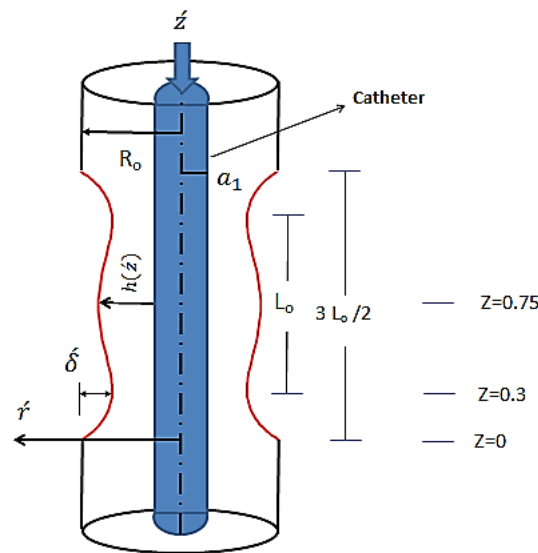


**Figure 1.** Problem modeling.

The stenosis frame can be prescribed as:

$$h(z') = \left\langle R_0 - \delta' z' \left( 11 - \frac{94z'}{3L_0} + \frac{32}{L_0^2} z'^2 - \frac{32}{3L_0^3} z'^3 \right) \right\rangle, \tag{1}$$

where  $L_0$  is the tube length and  $z'$  is the axial coordinate.

The governing equations to the nanofluid when neglecting the inertia force of the nanoparticles can be considered as [38]:

Mass equation

$$\frac{1}{r'} \frac{\partial}{\partial r'} (r' u') + \frac{\partial}{\partial z'} (w') = 0. \tag{2}$$

Axial momentum

$$\begin{aligned} \rho_{nf} \left[ \frac{\partial w'}{\partial t'} + u' \frac{\partial w'}{\partial r'} + w' \frac{\partial w'}{\partial z'} \right] = & -\frac{\partial p'}{\partial z'} + \mu_{nf} \left( \frac{\partial^2 w'}{\partial r'^2} + \frac{1}{r'} \frac{\partial w'}{\partial r'} + \frac{\partial^2 w'}{\partial z'^2} \right) \\ & + g(\rho\gamma)_{nf} (T' - T_1) - \sigma_{nf} \beta_0^2 w' - \frac{\mu_{nf}}{k'} w'. \end{aligned} \tag{3}$$

Radial momentum

$$\rho_{nf} \left[ \frac{\partial u'}{\partial t'} + u' \frac{\partial u'}{\partial r'} + w' \frac{\partial u'}{\partial z'} \right] = -\frac{\partial p'}{\partial r'} + \mu_{nf} \left( \frac{\partial^2 u'}{\partial r'^2} + \frac{1}{r'} \frac{\partial u'}{\partial r'} - \frac{u'}{r'^2} + \frac{\partial^2 u'}{\partial z'^2} \right). \tag{4}$$

The energy equation can be denoted accordingly

$$(\rho c_p)_{nf} \left[ \frac{\partial T'}{\partial t'} + u' \frac{\partial T'}{\partial r'} + w' \frac{\partial T'}{\partial z'} \right] = K_{nf} \left[ \frac{\partial^2 T'}{\partial r'^2} + \frac{1}{r'} \frac{\partial T'}{\partial r'} + \frac{\partial^2 T'}{\partial z'^2} \right] + D + \sigma_{nf} \beta_0^2 w'^2, \tag{5}$$

where  $u'$  and  $w'$  are the velocity components,  $\mu_{nf}$  is the coefficient of dynamic viscosity of nanofluid,  $T'$  is the temperature,  $c_p$  is the specific heat at constant pressure, and  $K_{nf}$  is the thermo-conductivity of nanofluid.

The suggestion of Chu and Fang [3] for the slip boundary conditions on the wall and the catheter can be represented as:

$$w' = u_0 \pm \Omega \frac{\partial w'}{\partial r'}, \text{ at } r' = h(z'), \tag{6}$$

$$w' = -u_0 \pm \Omega \frac{\partial w'}{\partial r'}, \text{ at } r' = a_1, \tag{7}$$

$$T' = T_1, \text{ at } r' = h(z'), \text{ (isothermal condition)} \tag{8}$$

$$\frac{\partial T'}{\partial r'} = 0, \text{ at } r' = a_1, \text{ (adiabatic condition)} \tag{9}$$

where  $\Omega$  is the mean free path and  $r'$  is the radial coordinate,  $(w', u')$  denotes the fluid phase velocity components along  $(z', r')$  directions,  $\rho_f, \rho_s$  are the actual densities of the fluid and nanoparticulate phases,  $P'$  denotes the pressure,  $D$  is the heat source, and  $\phi$  is the volume fraction of the nanoparticles. An empirical relation for the nanofluid properties can be considered as [2]:

$$\mu_{nf} = \frac{\mu_f}{(1 - \phi)^{2.5}} \rho_{nf} = (1 - \phi)\rho_f + \phi\rho_s, \tag{10}$$

$$(\rho\gamma)_{nf} = (1 - \phi)(\rho\gamma)_f + \phi(\rho\gamma)_s, (\rho c_p)_{nf} = (1 - \phi)(\rho c_p)_f + \phi(\rho c_p)_s, \tag{11}$$

$$\frac{K_{nf}}{K_f} = \frac{(K_s + 2K_f) - 2\phi(K_f - K_s)}{(K_s + 2K_f) + \phi(K_f - K_s)}, \sigma_{nf} = (1 - \phi)\sigma_f + \phi\sigma_s, \tag{12}$$

where,  $\sigma_f, \sigma_s, \sigma_{nf}, K_f, K_s, K_{nf}$  are the electrical and thermal conductivity of fluid, nanoparticles, and nanofluid, respectively.

Setting the next nondimensional variables:

$$z = \frac{z'}{L_0}, r = \frac{r'}{R_0}, u = \frac{L_0 u'}{\delta' u_0}, w = \frac{w'}{u_0}, Re = \frac{\rho_f u_0 L_0}{\mu_f}, \delta = \frac{\delta'}{R_0},$$

$$p = \frac{R_0^2}{\mu_f u_0 L_0} p', \varepsilon = \frac{R_0}{L_0}, t = \frac{u_0 t'}{R_0}, \theta = \frac{T' - T_1}{T_0 - T_1}, Ha = \sqrt{\frac{\sigma_f}{\mu_f}} \beta_0 R_0,$$

$$k = \frac{k'}{R_0^2}, Gr = \frac{g(\rho\gamma)_f R_0^2 (T_0 - T_1)}{u_0 \mu_f}, Br = \frac{\mu_f u_0^2}{K_f (T_0 - T_1)}, Kn = \frac{\Omega}{R_0}$$

where  $Kn$  is the Knudsen number,  $\theta$  is the nondimensional temperature,  $k$  is the nondimensional permeability parameter,  $Ha$  is Hartman number,  $Re$  is the Reynolds number of nanofluid,  $Gr$  is the Grashof number,  $Br$  is the Brinkman number,  $T_1$  is the inner wall temperature, and  $T_0$  ambient air temperature.

The governing Equations (2)–(9) with the non-dimensional parameters can be changed to the following equations:

$$\frac{1}{r} \frac{\partial}{\partial r}(ru) + \frac{\partial}{\partial z}(w) = 0 \tag{13}$$

$$\frac{\rho_{nf}}{\rho_f} Re \left[ \varepsilon \frac{\partial w}{\partial t} + \varepsilon^2 \delta u \frac{\partial w}{\partial r} + \varepsilon^2 w \frac{\partial w}{\partial z} \right] = -\frac{\partial p}{\partial z} - Ha^2 \left( 1 - \varphi + \frac{\sigma_s}{\sigma_f} \right) w - \frac{1}{K(1-\varphi)^{2.5}} w + \frac{\mu_{nf}}{\mu_f} \left( \frac{\partial^2 w}{\partial r^2} + \frac{1}{r} \frac{\partial w}{\partial r} + \varepsilon^2 \frac{\partial^2 w}{\partial z^2} \right) + \frac{(\rho\gamma)_{nf}}{(\rho\gamma)_f} Gr \theta \tag{14}$$

$$\frac{\rho_{nf}}{\rho_f} Re \left[ \frac{u_0}{L_0^2} \delta \frac{\partial u}{\partial t} + \varepsilon^4 \delta^2 u \frac{\partial u}{\partial r} + \varepsilon^3 \delta w \frac{\partial u}{\partial z} \right] = -\frac{\partial p}{\partial r} + \frac{\mu_{nf}}{\mu_f} \left( \delta \frac{\partial^2 u}{\partial r^2} + \frac{\delta}{r} \frac{\partial u}{\partial r} - \delta \frac{u}{r^2} + \varepsilon \frac{\partial^2 u}{\partial z^2} \right) \tag{15}$$

$$Re \frac{\mu_f (\rho c_p)_{nf}}{\rho_f K_{nf}} \varepsilon \left[ \frac{\partial \theta}{\partial t} + \varepsilon \delta u \frac{\partial \theta}{\partial r} + \varepsilon w \frac{\partial \theta}{\partial z} \right] = \left( \frac{\partial^2 \theta}{\partial r^2} + \frac{1}{r} \frac{\partial \theta}{\partial r} + \varepsilon^2 \frac{\partial^2 \theta}{\partial z^2} \right) + S \frac{K_f}{K_{nf}} + Ha^2 \frac{K_f}{K_{nf}} Br \left( 1 - \varphi + \varphi \frac{\sigma_s}{\sigma_f} \right) w^2 \tag{16}$$

The dimensionless stenosis frame equation becomes:

$$h(z) = \left\langle 1 - \delta z \left( 11 - \frac{94z}{3L_0} + \frac{32}{L_0^2} z^2 - \frac{32}{3L_0^3} z^3 \right) \right\rangle. \tag{17}$$

**Solution Procedure**

Employing the long wavelength approach ( $\delta \ll 1, \varepsilon \approx 0(1)$ ) used in Shapiro et al. [39], the set equations which describe the flow through the stenosis shape can be expressed as:

Radial momentum equation

$$\frac{\partial p}{\partial r} = 0 \text{ thus } \frac{dp}{dz} = \frac{\partial p}{\partial z}. \tag{18}$$

Axial momentum equation

$$(1 - \varphi)^{2.5} \frac{dp}{dz} = \left[ \frac{\partial^2 w}{\partial r^2} + \frac{1}{r} \frac{\partial w}{\partial r} \right] - \left( Ha^2 (1 - \varphi)^{2.5} \left( 1 - \varphi + \varphi \frac{\sigma_s}{\sigma_f} \right) + \frac{1}{k} \right) w + (1 - \varphi)^{2.5} \frac{(\rho\gamma)_{nf}}{(\rho\gamma)_f} Gr \theta. \tag{19}$$

Energy equation

$$\left( \frac{\partial^2 \theta}{\partial r^2} + \frac{1}{r} \frac{\partial \theta}{\partial r} \right) + S \frac{K_f}{K_{nf}} + Ha^2 \left( 1 - \varphi + \varphi \frac{\sigma_s}{\sigma_f} \right) \frac{K_f}{K_{nf}} Br w^2 = 0. \tag{20}$$

The non-dimensional slip velocity and temperature conditions are:

$$w = 1 \pm Kn \frac{\partial w}{\partial r} \text{ at } r = h(z), \tag{21}$$

$$w = -1 \pm Kn \frac{\partial w}{\partial r} \text{ at } r = J, \tag{22}$$

$$\theta = 0, \text{ at } r = h(z), \tag{23}$$

$$\frac{\partial \theta}{\partial r} = 0, \text{ at } r = J, \tag{24}$$

The dimensionless parameters in the previous equations are:  $J = \text{catheter size} \left( J = \frac{a_1}{R_0} \right)$ ,  
 The expression of the velocity  $w$  can be obtained from the solution of the Equation (19),  
 by introducing the boundary conditions (21) and (22):

$$w = C_1 br_1 + C_2 br_2 - \frac{(1 - \varphi)^{2.5} \frac{dp}{dz} - A}{B}. \tag{25}$$

The stream function can be got from the relationship of the velocity accordingly:

$$w = \frac{1}{r} \frac{\partial \psi}{\partial r}, \tag{26}$$

$$\psi(z, r) = \int r w dr, \tag{27}$$

$$\begin{aligned} \psi(z, r) = & \frac{C_1}{\sqrt{B}} \left( r I_1(\sqrt{Br}) - J I_1(\sqrt{BJ}) \right) + \frac{C_2}{\sqrt{B}} \left( r K_1(\sqrt{Br}) - J K_1(\sqrt{BJ}) \right) \\ & + \frac{\left( (1-\varphi)^{2.5} \frac{dp}{dz} - A \right)}{2B} \left( J^2 - r^2 \right), \end{aligned} \tag{28}$$

where  $C_1, C_2$  are

$$C_1 = \frac{(bJ_2 - Kn q_4) \left( 1 + \frac{1}{B} \left( (1-\varphi)^{2.5} \frac{dp}{dz} - A \right) \right) - (bh_2 - Kn q_2) \left( -1 + \frac{1}{B} \left( (1-\varphi)^{2.5} \frac{dp}{dz} - A \right) \right)}{(bh_1 - Kn q_1)(bJ_2 - Kn q_4) - (bh_2 - Kn q_2)(bJ_1 - Kn q_3)},$$

$$C_2 = \frac{(bh_1 - Kn q_1) \left( -1 + \frac{1}{B} \left( (1-\varphi)^{2.5} \frac{dp}{dz} - A \right) \right) - (bJ_1 - Kn q_3) \left( 1 + \frac{1}{B} \left( (1-\varphi)^{2.5} \frac{dp}{dz} - A \right) \right)}{(bh_1 - Kn q_1)(bJ_2 - Kn q_4) - (bh_2 - Kn q_2)(bJ_1 - Kn q_3)},$$

From which,

$$br_1 = I_0(\sqrt{Br}) = 1 + \frac{Br^2}{4} + \frac{B^2 r^4}{64} + \dots,$$

$$br_2 = K_0(\sqrt{Br}) = -\ln\left(\frac{\sqrt{Br}}{2}\right) - \frac{Br^2 \ln\left(\frac{\sqrt{Br}}{2}\right)}{4} + \frac{(2 - 2\gamma)Br^2}{8} - \gamma + \dots,$$

$$bh_1 = I_0(\sqrt{Bh}), \quad bh_2 = K_0(\sqrt{Bh}), \quad bJ_1 = I_0(\sqrt{BJ}), \quad bJ_2 = K_0(\sqrt{BJ}),$$

$$q_1 = \frac{\partial bh_1}{\partial h}, q_2 = \frac{\partial bh_2}{\partial h}, q_3 = \frac{\partial bJ_1}{\partial J}, q_4 = \frac{\partial bJ_2}{\partial J}, B = Ha^2(1 - \varphi)^{2.5} \left( 1 - \varphi + \varphi \frac{\sigma_s}{\sigma_f} \right) + \frac{1}{k},$$

$$bh_{11} = \int h bh_1 dh, \quad bh_{22} = \int h bh_2 dh, \quad bJ_{11} = \int J bJ_1 dJ, \quad bJ_{22} = \int J bJ_2 dJ,$$

$$A = (1 - \varphi)^{2.5} \left( 1 - \varphi + \varphi \frac{(\rho\gamma)_s}{(\rho\gamma)_f} \right) Gr(-0.04712557038 J^2 \ln(h) + 0.02356278519 h^2).$$

Here,  $I_0$  is the modified Bessel function of the first kind with zero order.  
 $K_0$  is the modified Bessel function of the second kind with zero order.  
 Then, one can now obtain the pressure difference from the flow rate as;

$$Q = \int_J^h r w(z, r) dr, \tag{29}$$

$$\frac{dp}{dz} = \frac{\partial p}{\partial z} = \frac{\left( Q - \frac{(bj_2 - Kn q_4) + (bh_2 - Kn q_2)}{((bh_1 - Kn q_1)(bj_2 - Kn q_4) - (bj_1 - Kn q_3)(bh_2 - Kn q_2))} bh_{11} \right.}{\left. + \frac{((bj_2 - Kn q_4) - (bh_2 - Kn q_2))A}{B((bh_1 - Kn q_1)(bj_2 - Kn q_4) - (bj_1 - Kn q_3)(bh_2 - Kn q_2))} bh_{11} \right.}$$

$$\left. + \frac{((bh_1 - Kn q_1) - (bj_1 - Kn q_3))}{((bh_1 - Kn q_1)(bj_2 - Kn q_4) - (bj_1 - Kn q_3)(bh_2 - Kn q_2))} bh_{22} \right.}$$

$$\left. + \frac{((bh_1 - Kn q_1) - (bj_1 - Kn q_3))A}{B((bh_1 - Kn q_1)(bj_2 - Kn q_4) - (bj_1 - Kn q_3)(bh_2 - Kn q_2))} bh_{22} - \frac{Ah^2}{2B} \right.}$$

$$\left. + \frac{((bj_2 - Kn q_4) + (bh_2 - Kn q_2))A}{((bh_1 - Kn q_1)(bj_2 - Kn q_4) - (bj_1 - Kn q_3)(bh_2 - Kn q_2))} bJ_{11} \right.}$$

$$\left. - \frac{((bj_2 - Kn q_4) - (bh_2 - Kn q_2))A}{B((bh_1 - Kn q_1)(bj_2 - Kn q_4) - (bj_1 - Kn q_3)(bh_2 - Kn q_2))} bJ_{11} \right.}$$

$$\left. - \frac{(bh_1 - Kn q_1) + (bj_1 - Kn q_3)}{((bh_1 - Kn q_1)(bj_2 - Kn q_4) - (bj_1 - Kn q_3)(bh_2 - Kn q_2))} bJ_{22} \right.}$$

$$\left. - \frac{((bh_1 - Kn q_1) - (bj_1 - Kn q_3))A}{B((bh_1 - Kn q_1)(bj_2 - Kn q_4) - (bj_1 - Kn q_3)(bh_2 - Kn q_2))} bJ_{22} + \frac{A^2}{2B} \right)$$

$$(1 - \varphi)^{2.5} \left( \frac{B((bj_2 - Kn q_4) - (bh_2 - Kn q_2))}{B((bh_1 - Kn q_1)(bj_2 - Kn q_4) - (bj_1 - Kn q_3)(bh_2 - Kn q_2))} bh_{11} \right.}$$

$$\left. + \frac{((bh_1 - Kn q_1) - (bj_1 - Kn q_3))}{B((bh_1 - Kn q_1)(bj_2 - Kn q_4) - (bj_1 - Kn q_3)(bh_2 - Kn q_2))} bh_{22} \right.}$$

$$\left. - \frac{h^2}{2B} - \frac{((bj_2 - Kn q_4) - (bh_2 - Kn q_2))}{B((bh_1 - Kn q_1)(bj_2 - Kn q_4) - (bj_1 - Kn q_3)(bh_2 - Kn q_2))} bJ_{11} \right.}$$

$$\left. - \frac{((bh_1 - Kn q_1) - (bj_1 - Kn q_3))}{B((bh_1 - Kn q_1)(bj_2 - Kn q_4) - (bj_1 - Kn q_3)(bh_2 - Kn q_2))} bJ_{22} + \frac{J^2}{2B} \right)$$

$$\Delta p = - \int_0^l \frac{dp}{dz} dz. \tag{30}$$

The expression of the temperature  $\theta$  obtained as the solution of Equation (20), subjected to temperature conditions (23) and (24) is:

$$\theta = L_1 + L_2 \ln(r) + \omega_1 + \omega_{21} + \omega_{22} + \omega_{23} + \omega_{24} + \omega_{25} + \omega_{26}, \tag{31}$$

$$L_1 = -L_2 \ln(h) - (\zeta_1 + \zeta_{21} + \zeta_{22} + \zeta_{23} + \zeta_{24} + \zeta_{25} + \zeta_{26}), \tag{32}$$

$$L_2 = -J(\vartheta_1 + \vartheta_{21} + \vartheta_{22} + \vartheta_{23} + \vartheta_{24} + \vartheta_{25} + \vartheta_{26}), \tag{33}$$

where:

$$\zeta_i = \theta p h_i = \theta p r_i|_{r=h}, \quad \vartheta_i = \left. \frac{\partial \theta p r_i}{\partial r} \right|_{r=J}, \quad \text{where } i = 1, 21, 22, 23, 24, 25, 26$$

$$\omega_1 = \theta p r_1 = -\frac{S r^2 K_f}{4 K_{nf}},$$

$$\omega_{21} = \theta p r_{21} = -EC_1^2 \left( \frac{r^2}{4} + \frac{B^2 r^6}{576} + \frac{B r^4}{32} + \frac{B^4 r^{10}}{409,600} + \frac{B^2 r^6}{1152} + \frac{B^3 r^8}{8192} \right)$$

$$\omega_{22} = \theta p r_{22} = -EC_2^2 \left\{ \left( \ln\left(\frac{\sqrt{B}}{2}\right) \right)^2 \left( \frac{r^2}{4} + \frac{B^2 r^6}{576} + \frac{B r^4}{32} \right) + 2 \ln\left(\frac{\sqrt{B}}{2}\right) \left( \frac{r^2}{4} (\ln(r) - 1) \right. \right.$$

$$\left. + \frac{B^2 r^6}{576} \left( \ln(r) - \frac{1}{3} \right) + \frac{B r^4}{32} \left( \ln(r) - \frac{1}{2} \right) \right) + \frac{r^2}{4} \left( (\ln(r))^2 - 2 \ln(r) + \frac{3}{2} \right)$$

$$\left. + \frac{B^2 r^6}{576} \left( (\ln(r))^2 - \frac{2}{3} \ln(r) + \frac{1}{6} \right) + \frac{B r^4}{32} \left( (\ln(r))^2 - \ln(r) + \frac{6}{16} \right) \right\}$$

$$\omega_{23} = \theta p r_{23} = -2E C_1 C_2 \left\{ \ln\left(\frac{\sqrt{B}}{2}\right) \left( -\frac{r^2}{4} - \frac{B^2 r^6}{576} - \frac{B r^4}{32} - \frac{B^2 r^6}{2304} - \frac{B^3 r^8}{16384} \right) \right.$$

$$\left. - \left( \frac{r^2}{4} (\ln(r) - 1) + \frac{B^2 r^6}{576} \left( \ln(r) - \frac{1}{3} \right) + \frac{B r^4}{32} \left( \ln(r) - \frac{1}{2} \right) \right) \right.$$

$$\left. - \frac{B^2 r^6}{2304} \left( \ln(r) - \frac{1}{3} \right) - \frac{B^3 r^8}{16384} \left( \ln(r) - \frac{1}{4} \right) \right\}$$

$$\omega_{24} = \theta p r_{24} = 2mEC_1 \left( \frac{r^2}{4} + \frac{B^2 r^6}{2304} + \frac{B r^4}{64} \right),$$

$$\omega_{25} = \theta pr_{25} = -2mEC_2 \left( \frac{r^2}{4} \ln \left( \frac{\sqrt{B}}{2} \right) + \frac{r^2}{4} (\ln(r) - 1) + \frac{Br^4}{64} \left( \ln \left( \frac{\sqrt{B}}{2} \right) + (\ln(r) - \frac{1}{2}) \right) \right)$$

$$\omega_{26} = \theta pr_{26} = -\frac{m^2 Er^2}{4}$$

$$m = \frac{\left( (1 - \varphi)^{2.5} \frac{dp}{dz} - A \right)}{B}, \quad E = Ha^2 \left( 1 - \varphi + \varphi \frac{\sigma_s}{\sigma_f} \right) \frac{K_f}{K_{nf}} Br$$

### 3. Results

#### 3.1. Validation of the Problem

Equations (25) and (33) represent the same formula as by Mekheimer [40], when neglecting the effect of nanoparticles on electrical conductivity, porosity, slip condition on the flow behavior, and the effect of magnetic field on the energy equation, Figure 2.

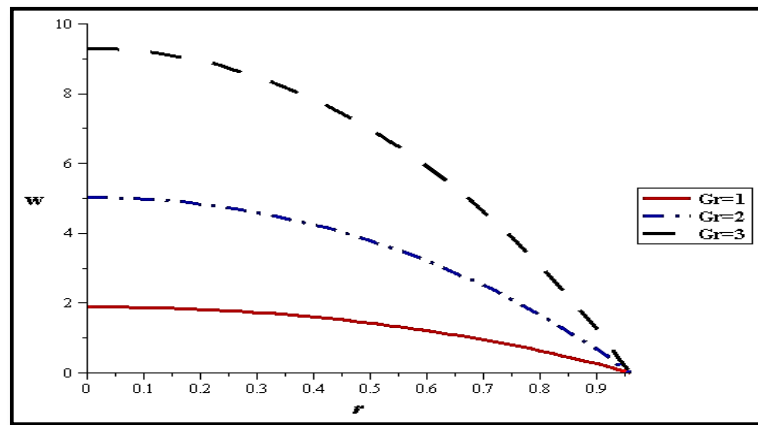


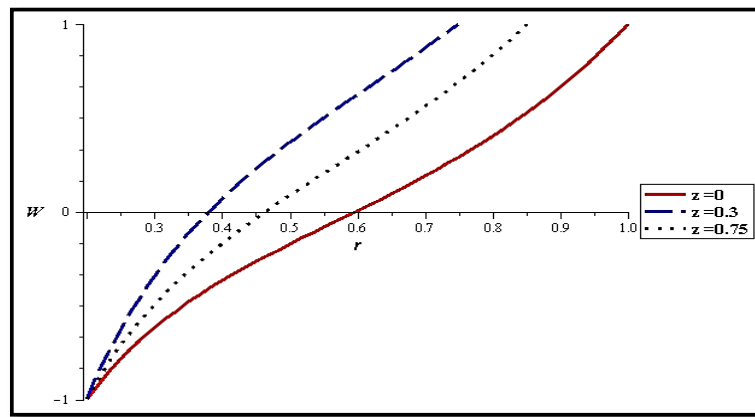
Figure 2. Velocity with different gravity at ( $Kn = 0, S = 0.1, k = 0.1, Ha = 1.5, J = 0, Q = 0.1, \delta = 0.05, \varphi = 0.02$ ).

#### 3.2. Numerical Analysis and Discussion

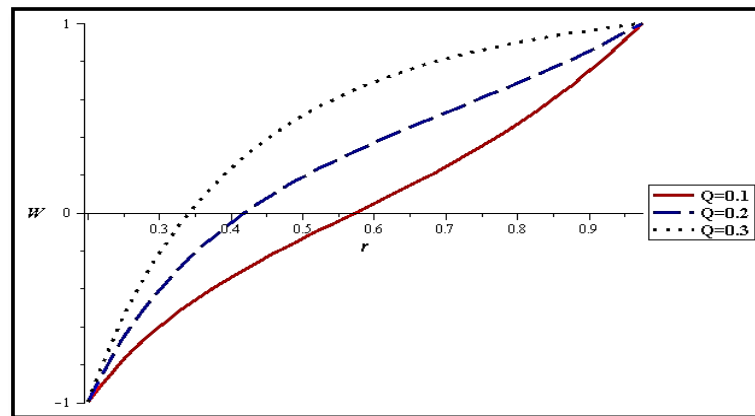
The influence of several parameters containing the nanoparticles concentration,  $\varphi$ , the catheter size,  $J$ , and the amplitude ratio of stenosis,  $\delta$  will be shown. The parameter values are chosen as:  $R_0$  (tube radius) = 12.5 mm;  $\varphi = 0, 0.02, 0.04, \text{ and } 0.05$ ;  $\delta = 0, 0.02 \text{ and } 0.04$ ;  $J = 0, 0.1, 0.2 \text{ and } 0.3$  [38]; and  $Q = 0.1, 0.2, \text{ and } 0.3$ . On the other hand, the results of the thermal study have been achieved through various flow rate ( $Q = 0.1, 0.2, 0.3$ ), catheter size ( $J = 0.1, 0.2, 0.3$ ), stenosis amplitude ratio ( $\delta = 0, 0.02, 0.04$ ), and nanoparticles concentration ( $\varphi = 0, 0.02, 0.04$ ).

Figure 3 displays the axial flow velocity at various positions. At  $z = 0.3$ , the reduced flow area causes the velocity to increase, while at  $z = 0$  the velocity decreases because of the growing cross section.

Figure 4 describes the velocity distributions for different flow rates, the velocity profiles show an increase of the centric velocity for the inflow rate near the wall but a decrease near the catheter because of the opposite direction of the catheter movement. The concentration effect of the nanoparticles on the velocity distribution is seen in Figure 5. Table 1 describes the small effect of nanoparticles concentration on the velocity distribution of the nanofluid.



**Figure 3.** Velocity at different locations at ( $Kn = 0$ ,  $Gr = 1$ ,  $\varphi = 0.02$ ,  $S = 0.1$ ,  $k = 0.1$ ,  $Ha = 10^{-5}$ ,  $J = 0.2$ ,  $Q = 0.1$ ,  $\delta = 0.02$ ).



**Figure 4.** Velocity with different flow rates at ( $Kn = 0$ ,  $\varphi = 0.02$ ,  $S = 0.1$ ,  $k = 0.1$ ,  $Ha = 10^{-5}$ ,  $J = 0.2$ ,  $\delta = 0.02$ ).

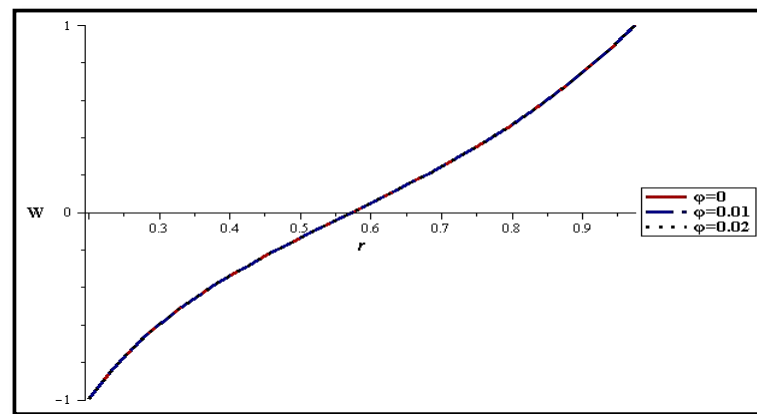
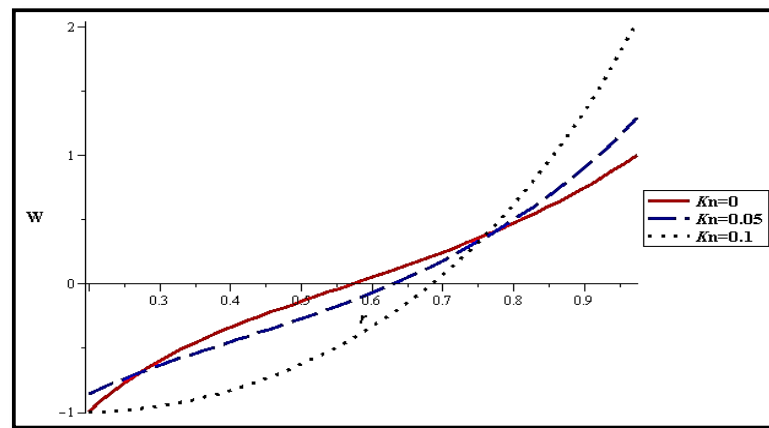


**Figure 5.** Velocity with different nanoparticles concentrations at ( $Kn = 0$ ,  $S = 0.1$ ,  $k = 0.1$ ,  $Ha = 10^{-5}$ ,  $J = 0.2$ ,  $Q = 0.2$ ,  $\delta = 0.02$ ).

**Table 1.** Velocity with different nanoparticles concentrations at ( $Kn = 0, S = 0.1, k = 0.1, Ha = 10^{-5}, J = 0.2, Q = 0.2, \delta = 0.02$ ).

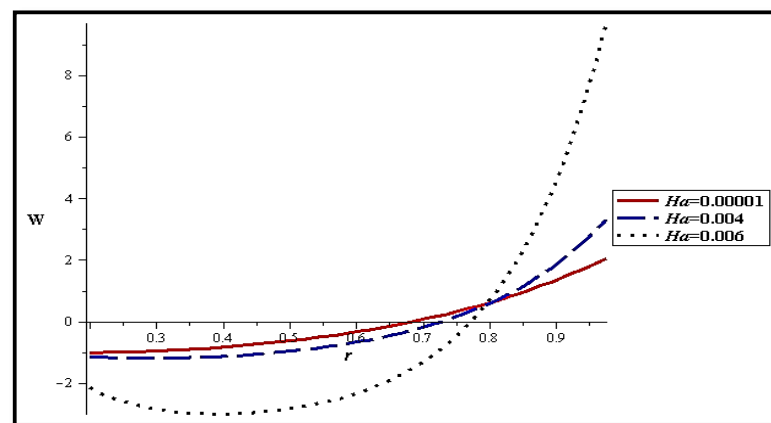
Radial ( $r$ )		Velocity ( $w$ )	
0.2	-1	-1	-1
0.3	-0.6028394149	-0.6028389455	-0.6028384998
0.4	-0.3424592848	-0.3424587957	-0.3424583314
0.5	-0.1391933897	-0.1391930735	-0.1391927738
0.6	0.0469001562	0.0469002316	0.0469003025
0.7	0.2419012707	0.2419011186	0.2419009731
0.8	0.4672595276	0.4672592396	0.4672589629
0.9	0.7443480614	0.7443478223	0.7443475934
1	1	1	1

Figure 6 investigates the influence of slip condition on fluid velocity profiles with a different Knudsen number. It is noticed that the near-wall velocity is enhanced due to the Knudsen number, while the Knudsen number at the catheter decreases the near-wall velocity, because the catheter moves in the opposite direction of the fluid at the inlet.



**Figure 6.** Velocity variations with  $Kn$  at ( $\varphi = 0.02, S = 0.1, k = 0.1, Ha = 10^{-5}, J = 0.2, Q = 0.1, \delta = 0.02$ ).

Figure 7 shows the fluid velocity with MHD at various magnetic fields. It was noted that the Hartman number within the tube wall increases the velocity at the wall, whilst the catheter velocity is decreased close to the wall.



**Figure 7.** Velocity with  $Ha$  at ( $Kn = 0.1, \varphi = 0.01, S = 0.1, k = 0.1, J = 0.2, Q = 0.1, \delta = 0.02$ ).

Figure 8 shows that the velocity distributions are affected by the permeability parameter and that the porous media increases the velocity. The velocity increases with the catheter, as shown in Figure 9.

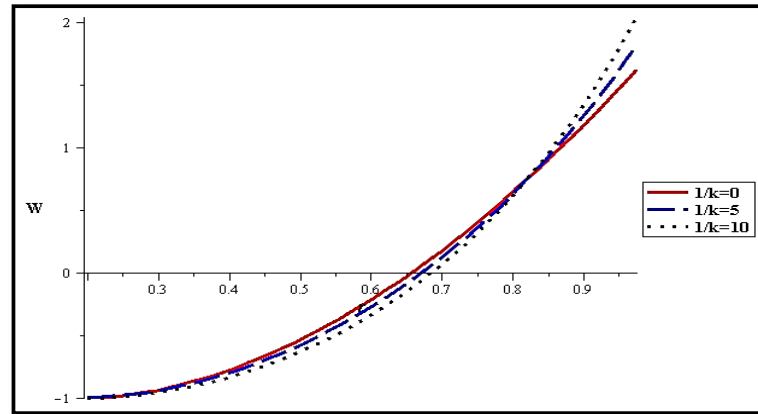


Figure 8. Velocity with porosity at ( $Kn = 0.1, \varphi = 0.01, S = 0.1, k = 0.1, Ha = 10^{-5}, J = 0.2, Q = 0.1, \delta = 0.02$ ).

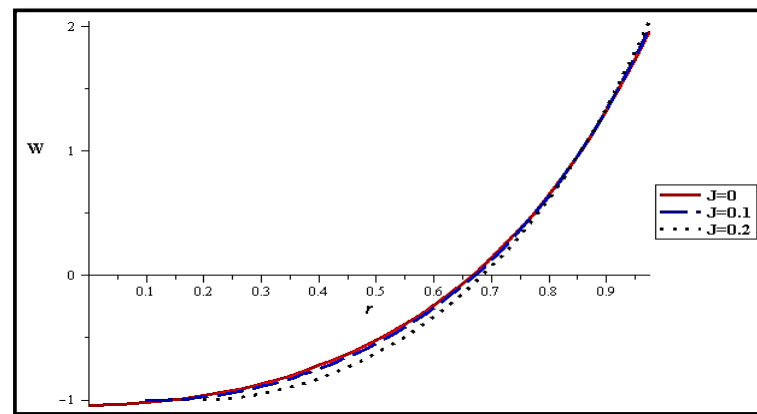


Figure 9. Velocity with catheter sizes at ( $Kn = 0.1, \varphi = 0.01, S = 0.1, k = 0.1, Ha = 10^{-5}, \delta = 0.02, Q = 0.1, Gr = 1$ ).

Figure 10 represents the relation between the amplitude ratio ( $\delta$ ) and the velocity distribution. The velocity decreases when the amplitude ratio ( $\delta$ ) increases. If the movement of the catheter is the same motion direction as the nanofluid at the wall of the artery stenosis, there is a symmetrical velocity distribution (see Figure 11). The influence of different values of the flow rate on the stream function is shown in Figure 12. The effect of the Knudsen number, porosity, and magnetic field is shown in Figures 13–15. It is observed that the streamlines are crowded with the flow rate.

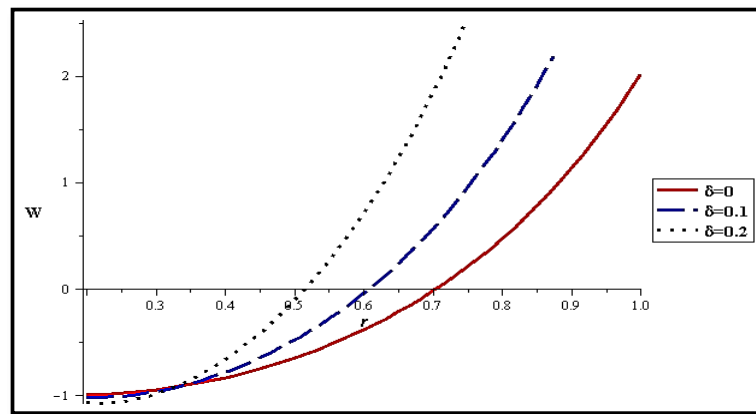


Figure 10. Velocity with different amplitude ratios at ( $Kn = 0.1, Ha = 10^{-5}, J = 0.2, \varphi = 0.01, S = 0.1, k = 0.1, Q = 0.1, Gr = 1$ ).

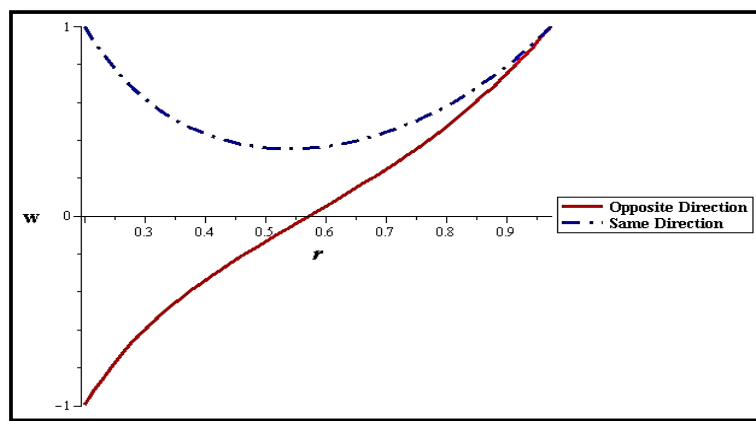


Figure 11. Velocity distribution with reverse catheter movement at ( $Kn = 0, Ha = 10^{-5}, J = 0.2, \varphi = 0.02, S = 0.1, k = 0.1, Q = 0.1, Gr = 1$ ).

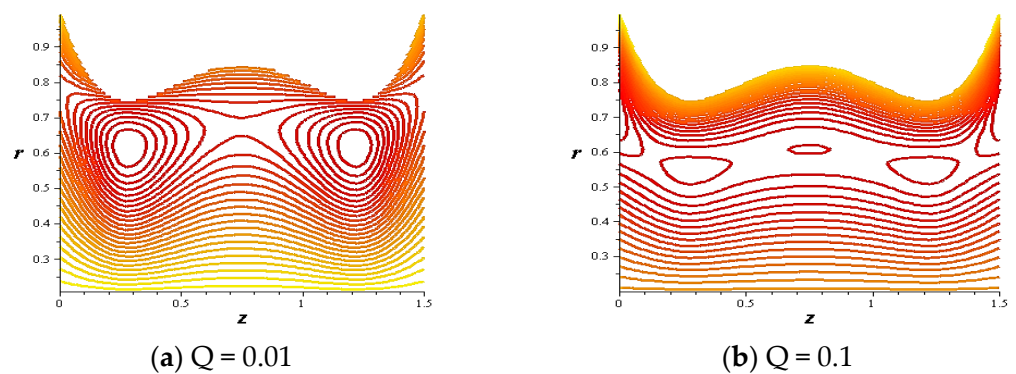
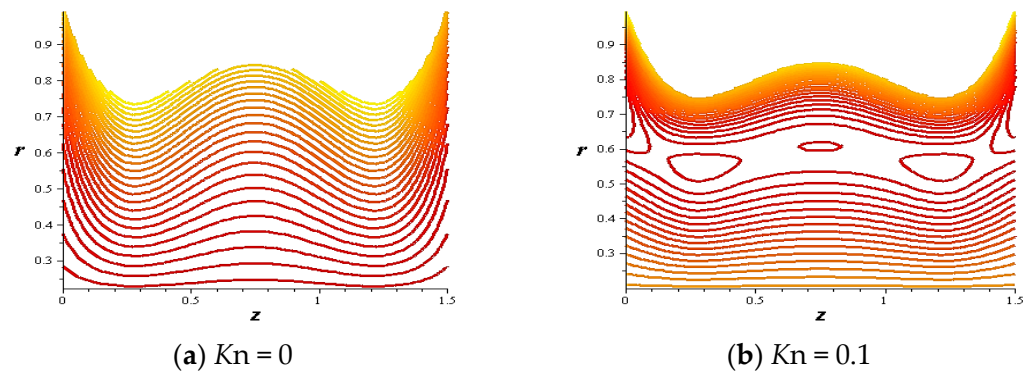
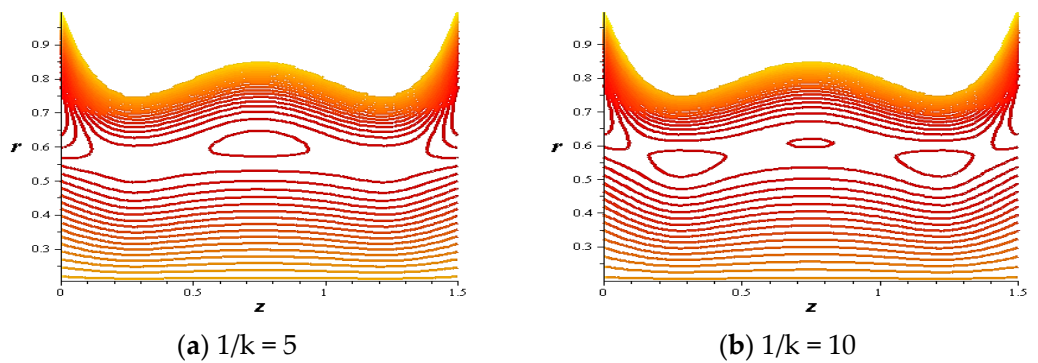


Figure 12. Streamlines with flow rate at ( $Kn = 0.1, J = 0.2, \varphi = 0.02, k = 0.1, \delta = 0.2, S = 0.1, Q = 0.1, Ha = 10^{-5}, Gr = 1$ ).



**Figure 13.** Streamlines with the Knudsen number at ( $J = 0.2, \varphi = 0.02, k = 0.1, \delta = 0.2, S = 0.1, Q = 0.1, Ha = 10^{-5}, Gr = 1$ ).



**Figure 14.** Streamlines with porosity at ( $Kn = 0.1, J = 0.2, \varphi = 0.02, \delta = 0.2, S = 0.1, Q = 0.1, Ha = 10^{-5}, Gr = 1$ ).

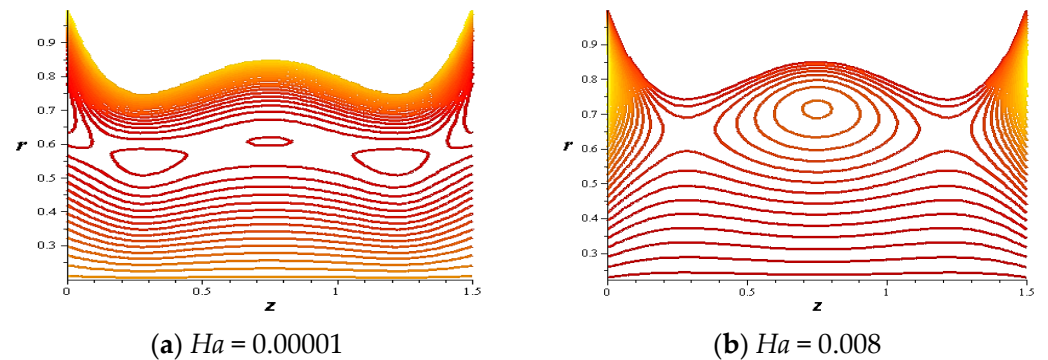


**Figure 15.** Streamlines with magnetic field at ( $Kn = 0.1, J = 0.2, \varphi = 0.02, k = 0.1, \delta = 0.2, S = 0.1, Q = 0.1, Gr = 1$ ).

Figure 16 shows the temperature gradient versus the locations. The flux rate has a significant role in promoting the temperature, in which the thermic energy increases with increasing flowing rate (see Figure 17). The temperature ( $\theta$ ) decreases with the concentration of nanoparticles ( $\varphi$ ), as seen in Figure 18, with the presence of Knudsen number.

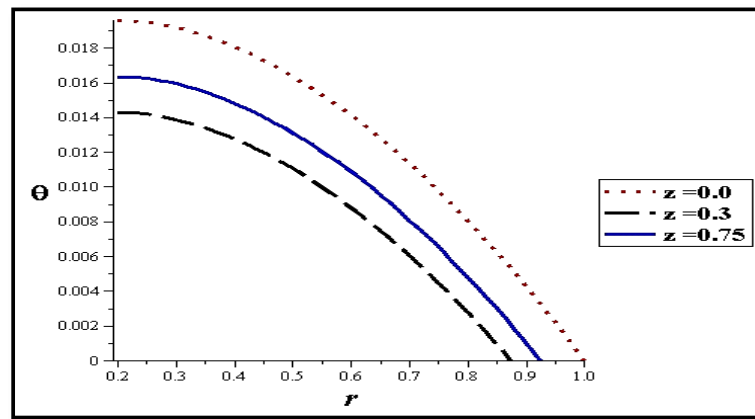


**Figure 16.** Temperature profiles with different locations at ( $Kn = 0.1, J = 0.2, \varphi = 0.02, \delta = 0.1, S = 0.1, Q = 0.1, Ha = 10^{-5}, Gr = 1, Br = 0.1, k = 0.1$ ).

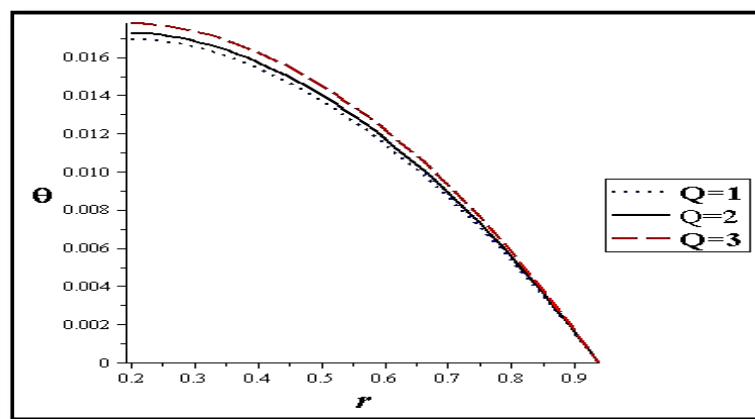


**Figure 17.** Temperature profiles with the flow rate at ( $Kn = 0.1, J = 0.2, \varphi = 0.02, \delta = 0.1, S = 0.1, Ha = 10^{-5}, Gr = 1, Br = 0.1, k = 0.1$ ).

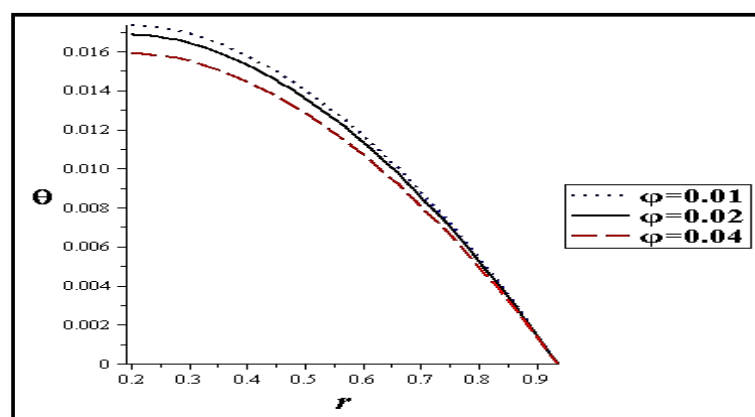


**Figure 18.** Temperature profiles with nanoparticles concentration at ( $Kn = 0.1, J = 0.2, \delta = 0.05, S = 0.1, Ha = 10^{-5}, Gr = 0.1, Br = 0.1, k = 0.1, Q = 0.1$ ).

The temperature is strongly affected by the magnetic field ( $Ha$ ), as shown in Figure 19, in which the temperature increases when increasing the magnetic field. With slipping, the presence of the catheter decreases the temperature (see Figure 20). Figure 21 shows the effect of stenosis amplitude ratio ( $\delta$ ) on the temperature, in which the temperature decreases when ( $\delta$ ) increases.

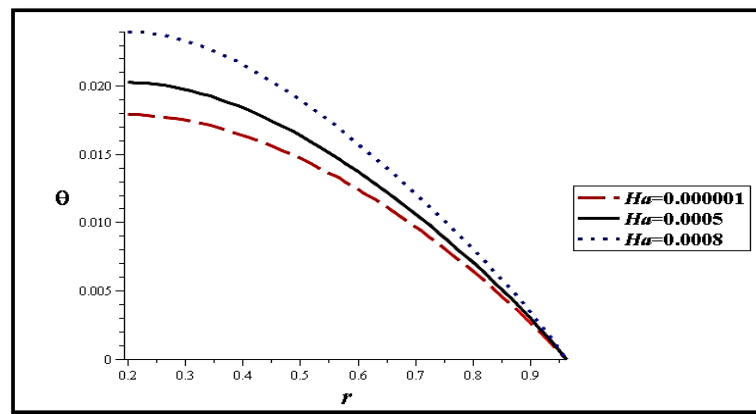


Figure 19. Temperature profiles with the Hartman number at ( $\varphi = 0.02, Kn = 0.1, J = 0.2, \delta = 0.05, S = 0.1, Gr = 0.1, Br = 0.1, k = 0.1, Q = 0.1$ ).

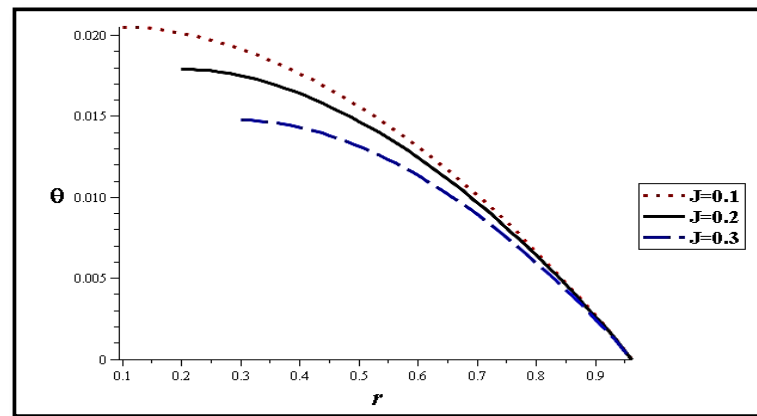


Figure 20. Temperature profiles with the catheter size at ( $\varphi = 0.02, Kn = 0.1, \delta = 0.05, S = 0.1, Gr = 0.1, Br = 0.1, k = 0.1, Q = 0.1, Ha = 10^{-5}$ ).

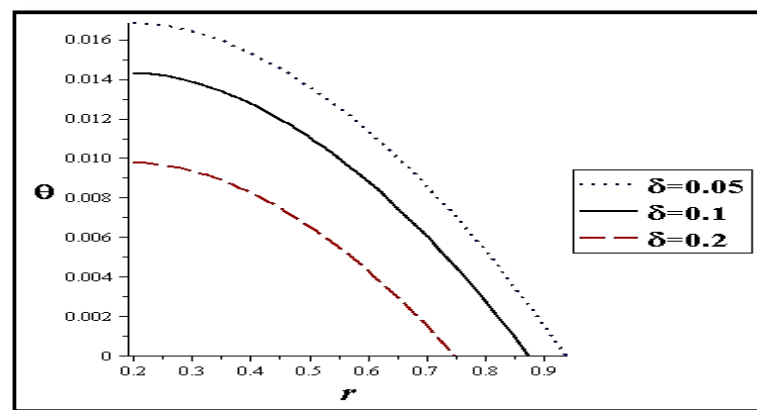
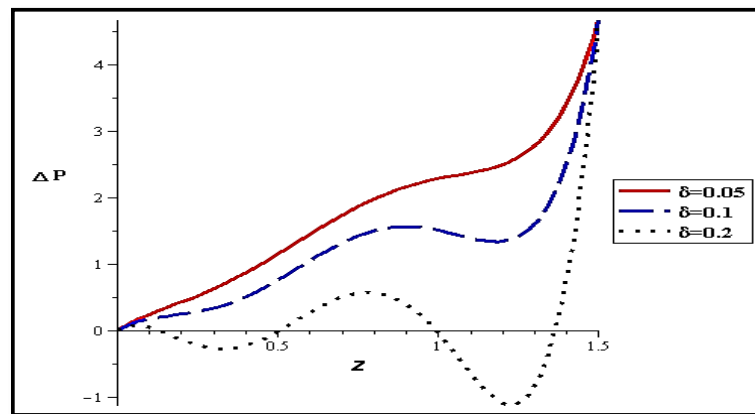
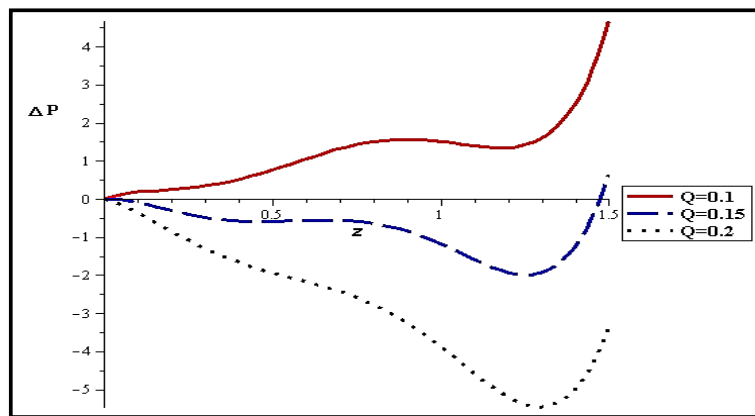


Figure 21. Temperature profiles with the amplitude ratio at ( $\varphi = 0.02, J = 0.2, Ha = 10^{-5}, Kn = 0.1, S = 0.1, Gr = 0.1, Br = 0.1, k = 0.1, Q = 0.1$ ).

The presence of amplitude ratio, flow rate, nanoparticles concentration, magnetic field, and Knudsen number increase the pressure difference, unlike the presence of catheter and gravity (see Figures 22–29).



**Figure 22.** Pressure difference profiles vs. positions at different amplitude ratios ( $\varphi = 0.02, J = 0.2, S = 0.1, Ha = 10^{-5}, Kn = 0, Gr = 1, k = 0.1, Q = 0.1$ ).



**Figure 23.** Pressure difference profiles vs. positions at different flow rates ( $\varphi = 0.02, \delta = 0.1, Ha = 10^{-5}, J = 0.2, Kn = 0, S = 0.1, Gr = 1, k = 0.1, Q = 0.1$ ).

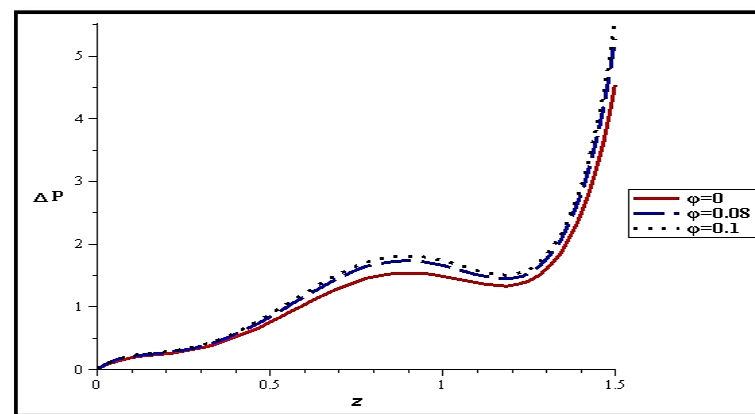


**Figure 24.** Pressure difference profiles vs. positions at different nanoparticle concentrations ( $\delta = 0.1, k = 0.1, Ha = 10^{-5}, J = 0.2, Kn = 0, S = 0.1, Gr = 1, Q = 0.1$ ).

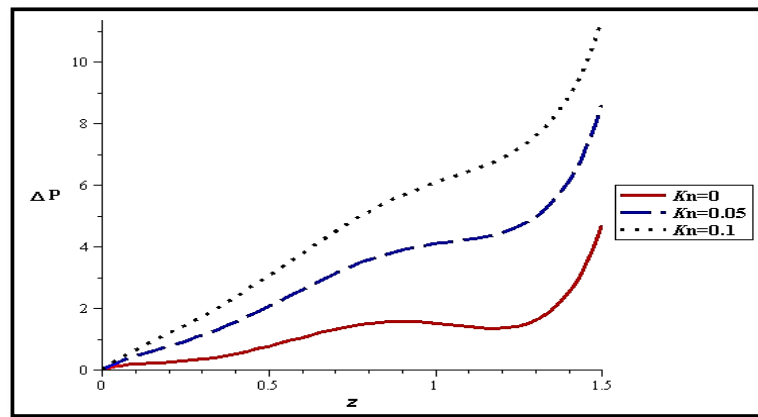


Figure 25. Pressure difference profiles vs. positions at different slip parameters ( $\varphi = 0.02$ ,  $\delta = 0.1$ ,  $J = 0.2$ ,  $Ha = 10^{-5}$ ,  $S = 0.1$ ,  $Gr = 1$ ,  $k = 0.1$ ,  $Q = 0.1$ ).

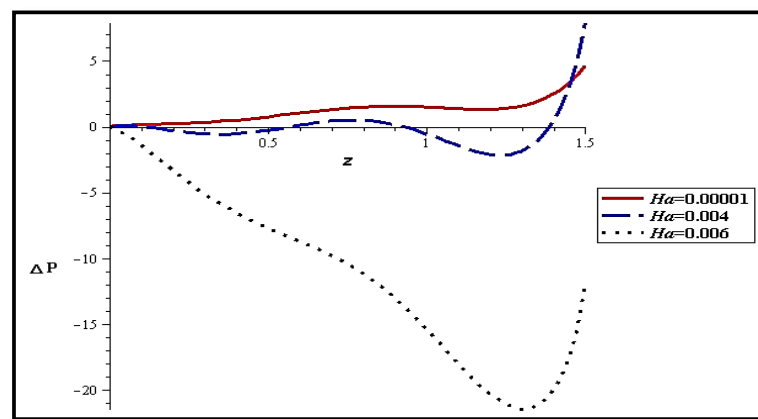


Figure 26. Pressure difference profiles vs. positions at different magnetic fields ( $Kn = 0$ ,  $\varphi = 0.02$ ,  $\delta = 0.1$ ,  $J = 0.2$ ,  $S = 0.1$ ,  $Gr = 1$ ,  $k = 0.1$ ,  $Q = 0.1$ ).

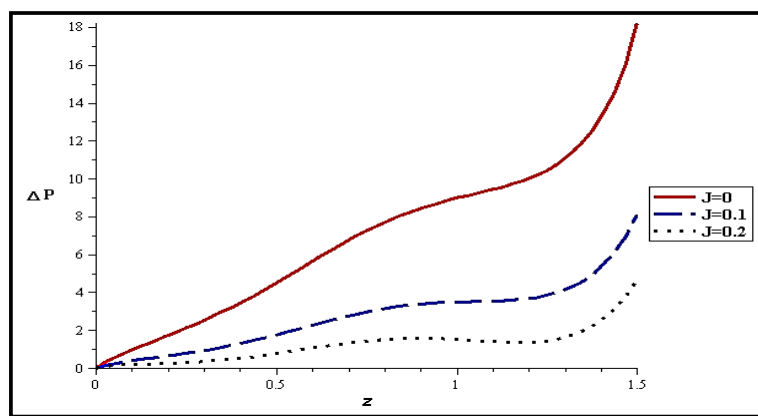
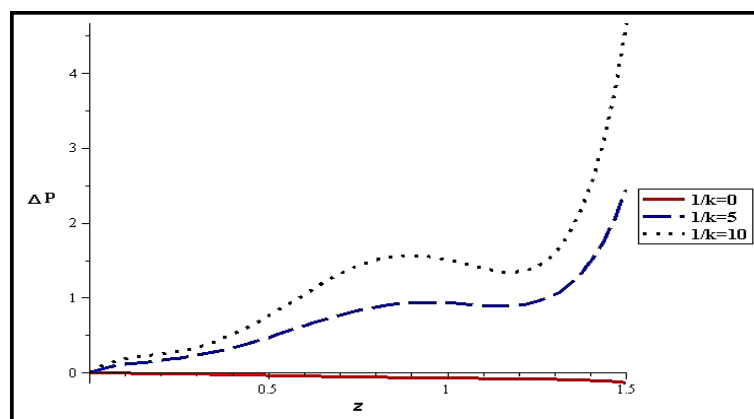
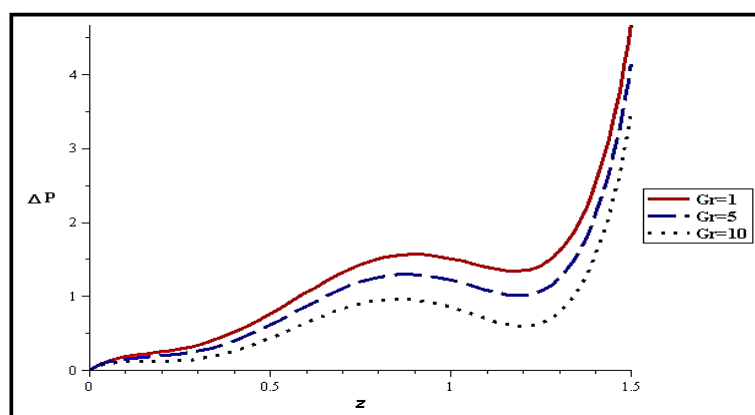


Figure 27. Pressure difference profiles vs. positions at different catheter sizes ( $Kn = 0$ ,  $\varphi = 0.02$ ,  $\delta = 0.1$ ,  $Ha = 10^{-5}$ ,  $S = 0.1$ ,  $Gr = 1$ ,  $k = 0.1$ ,  $Q = 0.1$ ).



**Figure 28.** Pressure difference profiles vs. positions at different porosities ( $Kn = 0$ ,  $\varphi = 0.02$ ,  $\delta = 0.1$ ,  $Ha = 10^{-5}$ ,  $S = 0.1$ ,  $Gr = 1$ ,  $J = 0.2$ ,  $Q = 0.1$ ).



**Figure 29.** Pressure difference profiles vs. positions at different gravity ( $Kn = 0$ ,  $\varphi = 0.02$ ,  $\delta = 0.1$ ,  $J = 0.2$ ,  $Ha = 10^{-5}$ ,  $S = 0.1$ ,  $k = 0.1$ ,  $Q = 0.1$ ).

#### 4. Conclusions

This paper analyzes the interaction effect of slip and thermal conditions on nanoparticle fluid suspension with a catheter in vertical stenotic artery with/without the presence of a magnetic field through porous media. The analytical method of settling has been investigated and used for exception, the velocity and temperature of the fluid for a regular tube with a long wavelength, and low Reynolds number approximation.

From the present study, the following points are noticed:

- Velocity increases within the curtailment, whilst during the extension, velocity decreases;
- The flowing rate boosts the velocity behind the artery wall and diminished it at the catheter;
- The nanoparticles concentration has a little effect on the velocity;
- With porous media the velocity increases at the catheter and decreases at the wall;
- The velocity increases when increasing the slipping and magnetic field at the wall;
- The temperature decreases within the contraction, whilst increasing within the expansion;
- The inflow rate and magnetic field enhance the thermal energy to the fluid unlike the presence of the catheter;
- The nanoparticles concentration, slipping, and porosity decrease the thermal energy;
- The presence of amplitude ratio, flow rate, nanoparticles concentration, magnetic field, and slipping increase the pressure difference, unlike the presence of catheter and gravity.

**Author Contributions:** Conceptualization, R.A. and I.M.E.; methodology, M.A. and R.A.; software, M.M.A. and R.A.; validation, M.M.A., and R.A.; formal analysis, M.A.; investigation, R.A.; resources, M.M.A. and R.A.; data curation, I.M.E.; writing—original draft preparation, R.A. and M.M.A.; writing—review and editing, R.A.; visualization, R.A. and I.M.E.; supervision, R.A. and M.A.; project administration, R.A. and K.M.; funding acquisition, K.M. All authors have read and agreed to the published version of the manuscript.

**Funding:** This research was funded by King Khalid University, grant number R.G.P.1/62/42.

**Institutional Review Board Statement:** The study was conducted in accordance with the Declaration of Helsinki and approved by the local ethics committee (Number 2021/015/52) at the Faculty of Engineering, Menoufia University, Shebin El-Kom, Egypt.

**Data Availability Statement:** Research data are not shared.

**Acknowledgments:** The authors extend their appreciation to the Deanship of Scientific Research at King Khalid University for funding this work through Research Group Project under grant number (R.G.P.1/62/42).

**Conflicts of Interest:** The authors declare no conflict of interest.

## References

1. Pal, S.L.; Jana, U.; Manna, P.K.; Mohanta, G.P.; Manavalan, R. Nanoparticle: An overview of preparation and characterization. *J. Appl. Pharm. Sci.* **2011**, *1*, 228–234.
2. Akbar, N.S.; Maraj, E.; Butt, A.W. Copper nanoparticles impinging on a curved channel with compliant walls and peristalsis. *Eur. Phys. J. Plus* **2014**, *129*, 183. [[CrossRef](#)]
3. Chu, W.K.-H.; Fang, J. Peristaltic transport in a slip flow. *Eur. Phys. J. B Condens. Matter Complex Syst.* **2000**, *16*, 543–547. [[CrossRef](#)]
4. Eldesoky, I.M. Slip effects on the unsteady MHD pulsatile blood flow through porous medium in an artery under the effect of body acceleration. *Int. J. Math. Math. Sci.* **2012**, *2012*, 860239. [[CrossRef](#)]
5. Eldesoky, I.M.; Kamel, M.H.; Abumandour, R.M. Numerical study of slip effect of unsteady MHD pulsatile flow through porous medium in an artery using generalized differential quadrature method (comparative study). In *The International Conference on Mathematics and Engineering Physics*; Military Technical College: Cairo, Egypt, 2014.
6. Abd Elnaby, M.A.; Haroun, M.H. A new model for study the effect of wall properties on peristaltic transport of a viscous fluid. *Commun. Nonlinear Sci. Numer. Simul.* **2008**, *13*, 752–762. [[CrossRef](#)]
7. Hasany, S.F.; Ahmed, I.; Rajan, J.; Rehman, A. Systematic review of the preparation techniques of iron oxide magnetic nanoparticles. *Nanosci. Nanotechnol.* **2012**, *2*, 148–158. [[CrossRef](#)]
8. Muthu, P.; Kumar, B.R.; Chandra, P. Peristaltic motion of micropolar fluid in circular cylindrical tubes: Effect of wall properties. *Appl. Math. Model.* **2008**, *32*, 2019–2033. [[CrossRef](#)]
9. Sreenadh, S.; Shankar, C.U.; Pallavi, A.R. Effects of wall properties and heat transfer on the peristaltic transport of food bolus through oesophagus—A mathematical model. *Int. J. Appl. Math. Mech.* **2012**, *8*, 93–108.
10. Hron, J.; Le Roux, C.; Malek, J.; Rajagopal, K. Flows of incompressible fluids subject to Navier’s slip on the boundary. *Comput. Math. Appl.* **2008**, *56*, 2128–2143. [[CrossRef](#)]
11. Abumandour, R.M.; Eldesoky, I.M.; Kamel, M.H.; Ahmed, M.M.; Abdelsalam, S.I. Peristaltic thrusting of a thermal-viscosity nanofluid through a resilient vertical pipe. *Z. Nat. A* **2020**, *75*, 727–738. [[CrossRef](#)]
12. Sharma, M.K.; Bansal, K.; Bansal, S. Pulsatile unsteady flow of blood through porous medium in a stenotic artery under the influence of transverse magnetic field. *Korea-Aust. Rheol. J.* **2012**, *24*, 181–189. [[CrossRef](#)]
13. Sucharitha, G.; Lakshminarayana, P.; Sandeep, N. MHD and Cross Diffusion Effects on Peristaltic Flow of a Casson Nanofluid in a Duct. *Appl. Math. Sci. Comput.* **2019**, *2*, 191–201.
14. Akbar, N.S. Metallic Nanoparticles Analysis for the Peristaltic Flow in an Asymmetric Channel with MHD. *IEEE Trans. Nanotechnol.* **2014**, *13*, 357–361. [[CrossRef](#)]
15. Sucharitha, G.; Vajravelu, K.; Lakshminarayana, P. Effect of heat and mass transfer on the peristaltic flow of a Jeffrey nanofluid in a tapered exible channel in the presence of aligned magnetic field. *Eur. Phys. J. Spec. Top.* **2019**, *228*, 2713–2728. [[CrossRef](#)]
16. Bejan, A. Entropy generation minimization: The new thermodynamics of finite-size devices and finite-time processes. *J. Appl. Phys.* **1996**, *79*, 1191–1218. [[CrossRef](#)]
17. Khan, W.A.; Ali, M. Recent developments in modeling and simulation of entropy generation for dissipative cross material with quartic autocatalysis. *Appl. Phys. A* **2019**, *125*, 397. [[CrossRef](#)]
18. Rashidi, M.M.; Bhatti, M.M.; Abbas, M.A.; Ali, M.E.-S. Entropy generation on MHD blood flow of nanofluid due to peristaltic waves. *Entropy* **2016**, *18*, 117. [[CrossRef](#)]
19. Hayat, T.; Rafiq, M.; Ahmad, B.; Asghar, S. Entropy generation analysis for peristaltic flow of nanoparticles in a rotating frame. *Int. J. Heat Mass Transf.* **2017**, *108*, 1775–1786. [[CrossRef](#)]

20. Ranjit, N.K.; Shit, G.C. Entropy generation on electroosmotic flow pumping by a uniform peristaltic wave under magnetic environment. *Energy* **2017**, *128*, 649–660. [[CrossRef](#)]
21. Ali, M.; Khan, W.A.; Irfan, M.; Sultan, F.; Shahzed, M.; Khan, M. Computational analysis of entropy generation for cross-nanofluid flow. *Appl. Nanosci.* **2019**, *10*, 3045–3055. [[CrossRef](#)]
22. Borges, M.E.; Sierra, M.; Cuevas, E.; García, R.; Esparza, P. Photocatalysis with solar energy: Sunlight-responsive photocatalyst based on TiO<sub>2</sub> loaded on a natural material for wastewater treatment. *Sol. Energy* **2016**, *135*, 527–535. [[CrossRef](#)]
23. Zhang, H.; Yang, H.; Chen, H.; Du, X.; Wen, D.; Wu, H. Photothermal conversion characteristics of gold nanoparticles under different filter conditions. *Sol. Energy* **2014**, *100*, 141–147. [[CrossRef](#)]
24. Zeiny, A.; Jin, H.; Bai, L.; Lin, G.; Wen, D. A comparative study of direct absorption nanofluids for solar thermal applications. *Sol. Energy* **2018**, *161*, 74–82. [[CrossRef](#)]
25. Shi, L.; He, Y.; Wang, X.; Hu, Y. Recyclable photo-thermal conversion and purification systems via Fe<sub>3</sub>O<sub>4</sub>@TiO<sub>2</sub> nanoparticles. *Energy Convers. Manag.* **2018**, *171*, 272–278. [[CrossRef](#)]
26. Prakash, J.; Siva, E.; Tripathi, D.; Kuharat, S.; Bég, O.A. Peristaltic pumping of magnetic nanofluids with thermal radiation and temperature-dependent viscosity effects: Modelling a solar magneto-biomimetic nanopump. *Renew. Energy* **2018**, *133*, 1308–1326. [[CrossRef](#)]
27. Prakash, J.; Ramesh, K.; Tripathi, D.; Kumar, R. Numerical simulation of heat transfer in blood flow altered by electroosmosis through tapered micro-vessels. *Microvasc. Res.* **2018**, *118*, 162–172. [[CrossRef](#)] [[PubMed](#)]
28. Hina, S.; Mustafa, M.; Hayat, T.; Alsaedi, A. Peristaltic transport of Powell–Eyring fluid in a curved channel with heat/mass transfer and wall properties. *Int. J. Heat Mass Transf.* **2016**, *101*, 156–165. [[CrossRef](#)]
29. Kumar, M.A.; Sreenadh, S.; Srinivas, A.N.S. Effects of wall properties and heat transfer on the peristaltic transport of a Jeffrey fluid in a channel. *Adv. Appl. Sci. Res.* **2013**, *6*, 156–172.
30. Reddy, M.G. Heat and mass transfer on magnetohydrodynamic peristaltic flow in a porous medium with partial slip. *Alex. Eng. J.* **2016**, *55*, 1225–1234. [[CrossRef](#)]
31. Suganya, S.; Muthamilselvan, M.; Al-Amri, F.; Abdalla, B. An exact solution for unsteady free convection flow of chemically reacting Al<sub>2</sub>O<sub>3</sub>-SiO<sub>2</sub>/Water hybrid nanofluid. *J. Mech. Eng. Sci.* **2020**, *235*, 3749–3763. [[CrossRef](#)]
32. Hayat, T.; Shafique, M.; Tanveer, A.; Alsaedi, A. Magnetohydrodynamic effects on peristaltic flow of hyperbolic tangent nanofluid with slip conditions and Joule heating in an inclined channel. *Int. J. Heat Mass Transf.* **2016**, *102*, 54–63. [[CrossRef](#)]
33. Ramesh, K.; Devakar, M. Magnetohydrodynamic peristaltic transport of couple stress fluid through porous medium in an inclined asymmetric channel with heat transfer. *J. Magn. Magn. Mater.* **2015**, *394*, 335–348. [[CrossRef](#)]
34. Hayat, T.; Farooq, S.; Alsaedi, A.; Ahmad, B. Hall and radial magnetic field effects on radiative peristaltic flow of Carreau–Yasuda fluid in a channel with convective heat and mass transfer. *J. Magn. Magn. Mater.* **2016**, *412*, 207–216. [[CrossRef](#)]
35. Misra, J.; Mallick, B.; Sinha, A. Heat and mass transfer in asymmetric channels during peristaltic transport of an MHD fluid having temperature-dependent properties. *Alex. Eng. J.* **2018**, *57*, 391–406. [[CrossRef](#)]
36. Hayat, T.; Riaz, A.; Tanveer, A.; Alsaedi, A. Peristaltic transport of tangent hyperbolic fluid with variable viscosity. *Therm. Sci. Eng. Prog.* **2018**, *6*, 217–225. [[CrossRef](#)]
37. Shaheen, A.; Asjad, M.I. Peristaltic flow of a Sisko fluid over a convectively heated surface with viscous dissipation. *J. Phys. Chem. Solids* **2018**, *122*, 210–217. [[CrossRef](#)]
38. Kothandapani, M.; Srinivas, S. On the influence of wall properties in the MHD peristaltic transport with heat transfer and porous medium. *Phys. Lett. A* **2008**, *372*, 4586–4591. [[CrossRef](#)]
39. Shapiro, A.H.; Jaffrin, M.Y.; Weinberg, S.L. Peristaltic pumping with long wavelengths at low Reynolds number. *J. Fluid Mech.* **1969**, *37*, 799–825. [[CrossRef](#)]
40. Mekheimer, K.S.; Mohamed, M.S.; Elnaqeeb, T. Metallic nanoparticles influence on blood flow through a stenotic artery. *Int. J. Pure Appl. Math.* **2016**, *107*, 201. [[CrossRef](#)]